www.ijarp.com ISSN 2456-9992 Page: 01-17

International Journal Advanced Research Publications

Review Article

Volume: 02
Issue: 06

STRUCTURE AND THERMOELECTRIC CHARACTERIZATIONS OF PEROVSKITE-BASED MATERIALS FOR HIGH TEMPERATURE POWER GENERATION

Adindu C. Iyasara[1*], Geoffrey O. Okafor[2], John N. Nweke[3], Dumpe K. Barinem[4], Nobert O. Osonwa[1], Henry I. Eneh[4], Ikechukwu C. Agha [4], Ngozi F. Okereke[5], Patrick O. Nwosibe[5], Arinzechukwu S. Okolo[6], Muhammed O. Ibrahim[7]

[1]Department of Ceramic and Glass Technology, AkanuIbiam Federal Polytechnic, Unwana, Nigeria.

[2]Department of Mechanical Engineering Technology, AkanuIbiam Federal Polytechnic, Unwana, Nigeria.

[3]Department of Electrical/Electronics Engineering Technology, AkanuIbiam Federal Polytechnic, Unwana, Nigeria.

[4]Department of Mechanical Engineering Technology, Federal Polytechnic, Ngodo, Isiochi, Nigeria.

[5]Department of Petroleum and Gas Engineering, Federal Polytechnic, Ngodo, Isiochi, Nigeria.

[6]Department of leadership and Management-project Management, University of Derby, United Kingdom.

[7]Department of Electrical/Electronics Engineering Technology, Federal Polytechnic, Nyak, Shedam, Nigeria.

Article Received: 21 May 2026, Article Revised: 9 June 2026, Published on: 29 June 2026

***Corresponding Author: Adindu C. Iyasara**

Department of Ceramic and Glass Technology, AkanuIbiam Federal Polytechnic, Unwana, Nigeria.

Doi: https://doi-doi.org/101555/ijarp.4181

ABSTRACT

Perovskite-based materials have attracted extensive attention for high-temperature thermoelectric power generation because of their excellent thermal stability, structural flexibility, environmental compatibility, and resistance to oxidation at elevated temperatures. The perovskite ABO_3 crystal structure accommodates a broad range of cation substitutes and oxygen defects, enabling effective tuning of electronic transport and phonon scattering mechanisms required for thermoelectric energy conversion. This work emphasizes the

structural and thermoelectric characterization methodologies used to establish the relationship between compositions, microstructure and transport behavior in perovskite thermoelectrics. Particle size analysis (PSA) is employed to evaluate powder finenessand distribution, which influence densification and grain growth. Thermogravimetric analysis (TGA) provides information on thermal decomposition, phase evolution and oxygen stability during heating. X-ray diffraction (XRD) is used for phase identification, lattice parameter determination, crystallite-size analysis, and structural refinement. Scanning electron microscopy (SEM) reveals grain morphology, porosity and microstructural homogeneity, while energy dispersive x-ray spectroscopy (EDS/EDX) confirms elemental composition and dopant distribution. The integration of these techniques provides a comprehensive understanding of crystal structure and microstructure affect thermoelectric properties at high temperatures. Representative Perovskite material (La-Sm doped strontium titanate) is discussed to illustrate current advances in oxide thermoelectrics for waste heat recovery and sustainable power generation.

KEYWORDS: Perovskite, thermoelectric, X-ray diffraction, crystal structure, phonon scattering.

1. INTRODUCTION

The increasing global demand for sustainable and efficient energy systems has intensified research into technologies capable of converting waste heat directly into electrical energy. Thermoelectric power generation is particularly attractive because it enables direct solid state conversion of thermal energy into electricity through the Seebeck effect without moving parts, chemical reactions, or greenhouse gas emissions during operation (Rowe, 2006; Snyder and Toberer, 2008). High temperature thermoelectric generators are especiallyimportant for recovering waste heat from industrial furnaces, automotive exhaust systems, gas turbines, petrochemical plants, and metallurgical operations.

Conventional thermoelectric materials such as bismuth telluride and lead telluride exhibit high thermoelectric performance but suffer from toxicity, scarcity, and poor thermal stability at elevated temperatures (Heremans, Dresselhaus, Bell and Morelli, 2013). Consequently, oxide thermoelectrics have emerged as promising alternatives because they possess superior oxidation resistance, thermal durability, and environmental compatibility. Perovskite oxides such as strontium titanate are among the most promising oxide thermoelectric materials due to their flexible ABO_3 crystal structure, which supports extensive cation substitution and defect engineering. These structural modifications strongly influence carrier concentration,

electronic band structure, and phonon transport thereby affecting thermoelectric efficiency (Pena and Fierro, 2001). Oxides generally have shown considerable potential for high-temperature power generation through defect engineering, donor doping and microstructural optimization.

The characterization of perovskite thermoelectrics therefore plays a critical role in understanding the relationship between processing, crystal structure, microstructure, and transport behavior. Techniques such as PSA, TGA, XRD, SEM and EDX provide essential information regarding powder characteristics, thermal stability, phase composition, grain morphology, and elemental homogeneity. These parameters strongly influence thermoelectric performance and long term stability under high temperature operating conditions.

This work presents a detailed experimental review of the structural and thermoelectric characterization of La +Sm doped $SrTiO_3$ perovskite based material for high temperature power generation with emphasizes on characterization methodologies.

2. STRUCTURAL CHARACTERIZATION

Structural characterization plays a critical role in the development and optimization of perovskite –based thermoelectric materials for high-temperature power generation. Comprehensive structural characterization commonly involves PSA, TGA, XRD, SEM and EDS/EDX. These techniques provide complementary information regarding powder characteristics, thermal stability, crystallographic structure, microstructure, and elemental composition.

2.1. Particle size analysis

Particle size analysis, PSAis one of the most important preliminary characterization techniques used in ceramic processing because the particle size and distribution of precursor powders strongly influence compaction, sintering behavior, densification, grain growth, and final thermoelectric performance (Rahaman, 2003). Several techniques are used for particle size determination including laser diffraction (LD), dynamic light scattering (DLS), sedimentation methods, sieve analysis and electron microscopy.

However, laser diffraction is the most widely used method for ceramic powder because it provides rapid and accurate measurement over a broad particle size range. LD particle size analyzer operates based on the scattering of laser light by suspended particles. Large particles scatter light at smaller angles, while smaller particles scatter light at wider angles. The particle size distribution is therefore calculated using Mie scattering theory or Fraunhofer diffraction theory.

Particle size distribution (PSD) to determine the particle diameters of the perovskite La+Sm doped $SrTiO_3$ was carried out using a Mastersizer 3000 laser particle size analyzer (Malven Limited, Worcestershire, UK). According to Basic Guide to Particle Characterization (2012),a typical Mastersizer 3000 is made up of three main systems[5]: optical bench; sample dispersion unit and instrument software. The optical bench is the measurement area through which the dispersed powder sample passes, and the laser beam illuminates the particles while the intensity of scattered light by the particles is accurately measured. The sample unit is designed to hold the sample (either wet or dry) and ensures that the correct concentration of the particles is channeled to the optical bench. The wet sample dispersion unit uses liquid dispersant, e.g. distilled water, while a dry sample dispersion unit suspends the sample in a flowing gas stream (dry air). The instrument software controls the system – controls the measurement process, analysis the scattering data generated and calculates the particle sizedistribution of the sample. A typical optical layout of a laser diffraction instrument is shown in Figure 1.

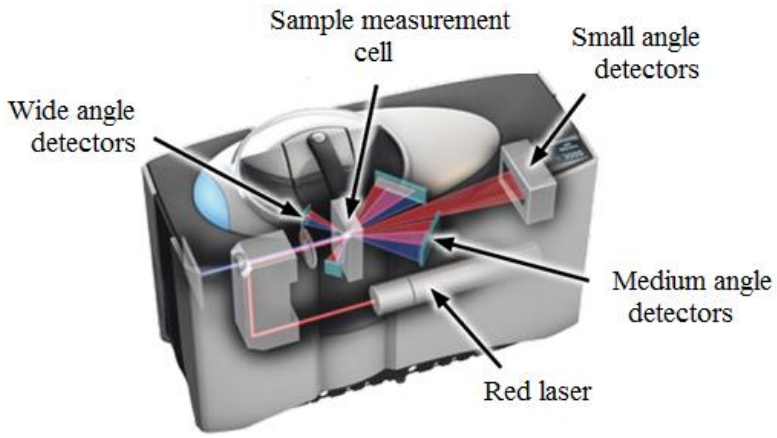

Figure 1. Schematic of a typical laser diffraction instrument showing the optical layout.

About 0.2 g of the perovskite La+Sm doped $SrTiO_3$ powder was dissolved in distilled water. After initializing the analyser, the background was measured, and the dissolved powder was dispersed into a 500 ml beaker filled with distilled water which was placed in the wet sample dispersion unit. The dispersed powder was de-agglomerated for about 30 seconds using the ultrasonic unit of the analyser. Finally, the measurement commenced and automatically measured particle size to an accuracy of ±0.001 μm.

As the beam passes through the dispersed particulate sample, the angular intensity of the scattered light relative to the beam was measured. The scattered data were collected and analysed by the instrument software. The size of the particles that created the scattering

pattern was calculated using the Mie theory of light scattering. The Mie theory requires the optical properties (mainly the refractive index) of both the dispersant and the measured sample. Five measurements on each sample were repeated and out of which the average particle diameter was determined. The particle size was reported as a volume equivalent sphere diameter. The uncertainty in the particle size distribution measurements using the laser diffraction Mastersizer 3000 analyser is as low as ±0.6 % while the repeatability in the data is ±0.5 %.

2.2. Thermogravimetric analysis

Thermogravimetric analysis, TGA (or simply thermogravimetry) is a branch of thermal analysis that studies the change in mass of a sample as a function of temperature or time when subjected to a controlled temperature and atmosphere (PerkinElmer, 2010). In TGA, a small quantity of sample is heated at a controlled rate while continuously monitoring weight changes. Mass variations occur due to dehydration, decomposition, oxidation, reduction, volatization, and oxygen release or absorption. The resulting thermogramprovides valuable information regarding thermal stability and reaction mechanisms.

TGA to determine the rate of oxygen uptake (weight variation) and thermal stability of the perovskite La+Sm doped $SrTiO_3$ samples in air at room temperature to 1000 ^oC was carried out using PerkinElmer Pyris 1 TGA (PerkinElmer Instruments, Norwalk, USA) computer-controlled analyser.The sample pan (supported with precision or microbalance) of the analyser operates with a high resolution (sensitivity) and can detect a mass change as small as 0.1 µg up to a maximum capacity of 1300 mg. The furnace uses Pt/30 % Rh elements and change in weight of the ceramic samples were measured in air with a 5 ^oC/min heating rate up to 1000 ^oC and a 5 ^oC/min cooling rate to room temperature.

2.3. X-Ray Diffraction

X-ray diffraction (XRD) is a non-destructive technique used for identification of crystalline materials (in powdered and solid forms), qualitative analysis and determination of the phases present (Cullity and Stock, 2001). X-rays are electromagnetic radiation with high frequency (~ 10^{18} Hz), low wavelength (~ 10^{-10} m = 1 Å) and energies in the range of 100 eV-1000 KeV. An anode (a major component of x-ray tube where the x-rays are produced) converts the energy of the electrons (electronic energy) into x-rays and dissipates the heat produced in the process. For an effective performance, the anode materials are required to be metallic (i.e. conduct electrons), possess high melting point and produce characteristic wavelengths of about 0.5 to 2.3 Å. Typical anodes are chromium (Cr), iron (Fe), cobalt (Co), copper (Cu) and

molybdenum (Mo) . A Cu anode is the most commonly used in powder diffraction since its wavelength (λ) is comparable with the inter-atomic distances (~ 1.5 Å) required in XRD while Mo is preferred in single crystal diffraction.

Crystal (lattice) planes are described by notations called Miller indices. The Miller indices refer to the reciprocal of the points at which a, b, and c axes of the lattice planes are intersected by the plane, denoted h, k, and l from a defined origin. These lattice planes are arranged in space to form a series of parallel planes which are separated from each other by an interplanar spacing d.When an x-ray beam of wavelength λ is incident on the crystal planes of a crystalline material at an angle θ, a constructive interference of the diffraction occurs when Bragg's law (Figure 2) is satisfied, i.e. when AC+BC is equal to a whole number of wavelength (nλ). Bragg's law is expressed as:

$$n\lambda = 2d\sin\theta \quad 1.0$$

where n is an integer representing the order of the diffraction peak. The signals generated are then converted into peaks (fingerprints) by the diffractometer.

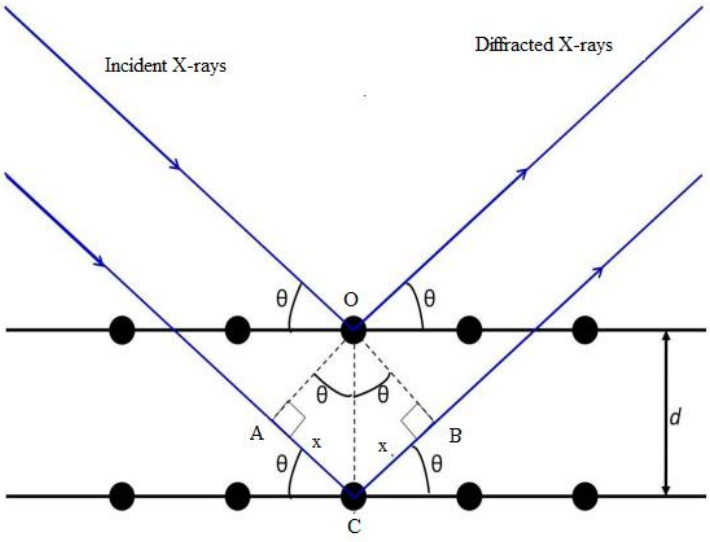

Figure 1. Schematic diagram of an X-ray beam interacting with crystal planes and illustrating Bragg's law.

In this work, the crystal structures of the crushed sintered La+Sm doped $SrTiO_3$ pellets were characterized by powder x-ray diffraction with Cu Kα radiation with λ = 1.5406 Å using Siemens D5000 x-ray diffractometer (Siemens Analytical X-ray Instruments Inc., Madison W1, 53719) operated with 40 kV voltage, and 40 mA current.

A specimen holder was filled with the powder sample and gently pressed down with a glass slide so that the top of the sample is on the same level with the top of the specimen holder. This simple precaution is necessary to prevent "specimen height displacement error". After loading the sample into the diffractometer, the scan was conducted across the 2θ range of 20 – 80 degrees with a step size of 0.01° or 0.02° at a scan rate of 1°/min. Phase identity and purity of the collected data were analysedusing the "Bruker Eva COD" and "ICDD Sleve+ PDF-4+" software (Graulis et al, 2009; Fawcett, Needham, Crowder, and Kabekkodu, 2009). The theoretical density, ρ_{th} was calculated from the equation below (West , 2014):

$$\rho_{th} = \frac{(FW*Z*1.66)}{V} \quad , \qquad 2.0$$

[

while the relative density, $\rho_r(\%)$ was determined from the experimental density over the theoretical density(Wang and Wang, 2013);

$$\rho_r = \frac{\rho_e}{\rho_{th}} * 100 \qquad 3.0$$

[

where: FW is formula weight of the sample (g/mol); Z is the number of atoms per unit cell and V is the cell or lattice volume of the sample ($Å^3$) which was calculated using the lattice parameter constants from XRD data of the crushed pellets. The errors associated with the calculation of lattice parameters are limited by specimen displacement, offset of 2Theta (2θ) degrees and peak position which amount to uncertainties of ±0.001 Å.

2.4. Scanning Electron Microscopy

A scanning electron microscope, SEM is an instrument used for the observation of solid specimen surfaces. According to Australian Microscopy & Microanalysis Research Facility online learning module (Myscope, 2014), SEM is a tool for seeing invisible worlds of microspace (1 micron = 10^{-6} m) and nanospace (1 nanometer = 10^{-9} m). SEM uses a focussed incident electron beam of high energy to generate a variety of emitted signals when it strikes the specimen surface. SEM uses these signals to observe, analyse and interpret information such as microstructure, chemical composition, morphology (texture) and topography (structural shape) of specimens at magnifications ranging from 10x to ~ 300,000x.

When the primary (incident) electron beam strikes the sample, it penetrates to a depth ~ 1 μm forming a limiting interaction volume from which several signals (radiations) are emitted as

shown in Figure 3(a).These signals include secondary electrons (SEs), backscattered electrons (BSEs), characteristic x-rays, cathodoluminescence (photons) and auger electrons. Secondary electrons (SEs) originate from the atoms of the sample and are released when electron beam interacts inelastically with lower energy shell of sample elements. The electrons are released from topmost regions (~ 15 nm) from the sample surface (Myscope, 2014). SEs have low energy (< 50 eV), and very useful for the inspection of the topography of the sample surface. However, BSEs originate from deeper regions of the sample and are reflected back after elastic interactions between the primary electron beam and the sample nucleus. Backscattered electrons show high sensitivity to atomic number of sample elements. The higher the atomic number (Z) of an element, the brighter the sample image appears. For example, iron, Fe atoms (Z = 26) scatter more electrons back towards the detector than the lighter aluminium, Al (Z =13) atoms, hence shows a brighter SEM image.

Typically, SEM consists of three main components (Myscope, 2014): a microscope column; ancillary equipment unit and the computer device. The microscope column contains the electron gun at the top, followed by the column, magnetic lens system and the specimen chamber at the base. The electron gun generates the electrons, while the "column" is the channel through which the electron beam travels. The magnetic lens system (comprising the condenser lenses, deflection, or scan coils and final or objective lenses) processes the electron beam by controlling its intensity and brings the electron into focus on the specimen. The specimen chamber houses the specimen and maintains a high vacuum condition in order to minimize scattering (attenuation) of the electron before reaching the specimen. Generally, the electron gun, lenses and specimen chamber must be under a high vacuum for an efficient operation of the SEM. This condition is expedient because an electron cannot freely travel through air.

The ancillary equipment unit includes the pump system (to keep the system under vacuum), water chilling system and the electron detectors. The water chilling system maintains the magnetic lenses at a constant temperature of 20 ^{o}C during the operation. When the chiller fails, the lenses heat up and the SEM will automatically shut down. Electron detectors collect the generated signals from the specimen. The collected signals are converted to photons using a scintillator, amplified in a photo multiplier, hence converted to electrical signals. The computer device drives the SEM and displays the image on the viewing screen. A simplified SEM operational set up is shown in Figure 3(b). The quality of an image produced in SEM is controlled by the properties of the sample, sample preparation technique

and instrumental parameters such as accelerating voltage scan speed, working distance and spot size.

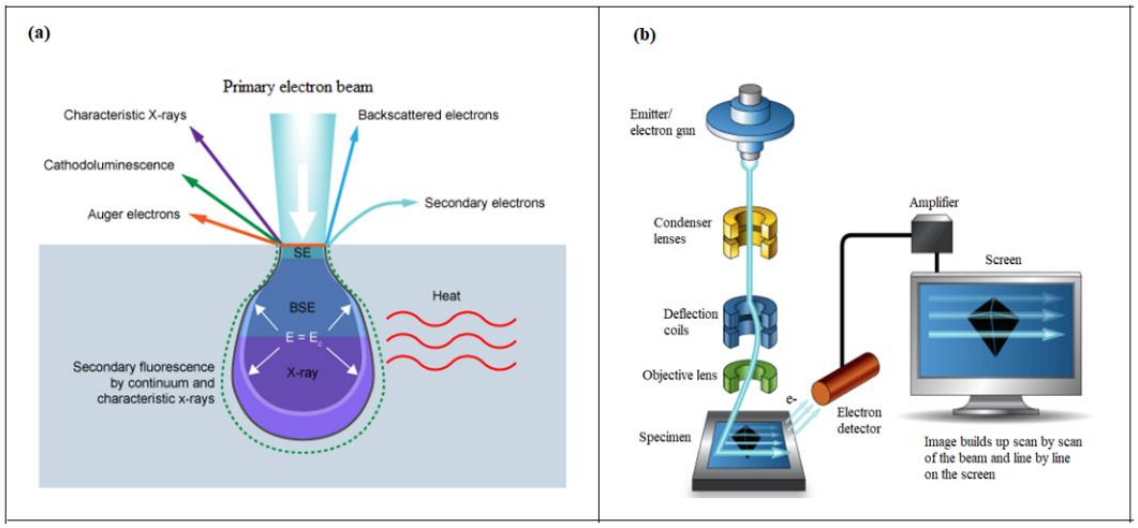

Figure 3.Schematics of (a) scanning electron microscope operational set-up and (b) Primary electron beam-Sample interaction (Myscope, 2014).

The perovskite La+Sm doped $SrTiO_3$ Samples for microstructural examination was prepared by grinding and polishing to a mirror finish on a diamond polishing wheel. The polished samples were thermally etched at 90 % of the sintering temperature in air or 5 % H_2/N_2 gas (depending on the processing atmosphere) for 30 minutes to reveal the grain structures. Thermally etched samples were mounted on aluminium pin-type stubs with adhesive tapes. The prepared samples were carbon coated using Edwards vacuum carbon coater (Edwards High Vacuum Ltd, England) to make them conductive and maximize secondary electron signal from the specimen. Conductive samples prevent “charging”. Charging is a build-up of negative charge at the point where the electron beam strikes the sample surface. Charging causes uncommon effects such as abnormal contrast and image deformation. The edges (sides) of the mounted samples are obviously poorly coated. Therefore, conductive silver-based paste (Agar Scientific Ltd, Stansted, UK) was applied on the edges. After carbon coating of the samples, the microstructures were examined using XL 30 S-FEG (Philips/FEI) at an accelerating voltage of 5-20 kV. Secondary electron images were obtained from the sample surfaces.

2.5 Energy Dispersive X-Ray Spectroscopy

Energy dispersive spectroscopy (EDX) is a chemical microanalysis technique linked to SEM to analyse characteristic x-ray spectra by measuring the energies of the x-rays. As the electron beam strikes the sample, the EDX technique detects the x-rays emitted and characterizes the elemental composition of the sample. The x-rays are generated within the whole region of the interaction volume as shown in Figure 3(a). As an electron is removed from the inner shell of the atom by the incident primary electron beam, the atom becomes ionized and unstable. The atom regains its stability when an electron from an outer shell fills the inner shell vacancy, and in so doing, x-ray photon is emitted. The energy of the emitted photon is characteristic of the energy difference between the two energy states for the atom (Brandon and Kaplan, 2008).

EDX system is made up of three major components; x-ray detector, pulse processor and analyser. The x-ray detector identifies and converts the x-rays into electronic signals while the pulse processor measures the electronic signals. In measuring the electronic signals, the energy of each x-ray is identified. The analyser finally displays and interprets the x-ray data.The data generated for collection consists of spectra with peaks corresponding to all the different elements that are present in the sample. The software (analyser) enables auto-identification of the peaks and calculation of the atomic percentage of the elements detected. These spectra together with the atomic percent of the elements confirmed in each of the samples are collected.

Sources of errors associated with EDX analysis are related to the sample, SEM, EDX detector and the data software **(**Myscope, 2014). Therefore, the accuracy of EDX analysis depends on the sum of all these errors, hence difficult to quantify. The combined uncertainties limit the precision of EDX analysis to ±2 % **(**Myscope, 2014).

In this work, the EDX analysis was performed using INCA Energy EDS X-ray Microanalysis System (Oxford Instruments Analytical, UK) comprised of INCA EDS detectors, INCAx-stream pulse processors and INCAEnergy software and linked to Philips XL 30 S-FEG SEM.

3. THERMOELECTRIC CHARACTERISATION

Thermoelectric characterization is essential for evaluating the suitability of perovskite based materials for high temperature power generation. The thermoelectric efficiency of these materials depends primarily on the Seebeck coefficient, electrical conductivity, and thermal conductivity which collectively determine the dimensionless figure of merit (ZT) (Snyder and Toberer, 2008). Accurate characterization of these transport parameters provides important

insight into carrier transport mechanisms, oxygen-vacancy behavior, phonon scattering, and the influence of crystal structure and microstructure on thermoelectric performance. A comprehensive thermoelectric characterization is required to establish the relationship between processing conditions, structure, and high-temperature behavior for perovskite thermoelectrics such as $SrTiO_3$ and other related materials.

3.1. Electrical Conductivity and Seebeck Coefficient

The electrical conductivity (σ) and Seebeck coefficient (S) of the perovskite La+Sm doped $SrTiO_3$ samples were measured simultaneously by employing the Van der Pauw four-point probe method (commonly known as four-point probe method). The four-point probe method was first proposed in 1916 by Frank Wenner to measure the earth's resistivity (Wenner,1916). It was later used by Valdes in 1954 for measuring semiconductor wafer resistivity (Valdes,1954). Four-point probe method is preferable to other conventional methods to measure the resistivity of low resistive (conductive) samples (Boston et al, 2016). It provides less internal resistance and a better accuracy. The four-point probe method involves bringing four-independent electrical terminals (probes) in contact with a sample surface of unknown resistance (Garcia-Vazquez ,2017). Two of the terminals (outer probes) are utilized for sourcing current (current contacts). A pre-set electrical current is passed through the outer probes from an external source. The other two terminals (inner probes) are used for measuring the resulting voltage drop (voltage contacts) across the surface of the sample. To obtain reliable data, the four-point probe method requires the sample to be homogeneous (devoid of holes or cavities) and flat (constant thickness) (Boor and Schmidt, 2011).

A rectangular-shaped La+Sm doped $SrTiO_3$ ceramic of about 20 mm in length, 3 mm in width and ≤ 2 mm in thickness or a circular-shaped pellet of 16 mm in diameter with ≤ 2 mm thickness was prepared for electrical conductivity and Seebeck coefficient measurements. The Van der Pauw four-point probe method was employed for the simultaneous measurements of the electrical conductivity and Seebeck coefficient under identical conditions using a Netzsch SBA 458 Nemesis (NETZSCH-Geratabau GmbH, Germany) Seebeck coefficient and electrical conductivity analyser. The instrument allows samples of different geometries (square, rectangle, round/disc and strips) to be measured The sample was placed with both ends on a sample support in the carrier system unit of the Nemesis measuring instrument. The carrier system enclosed in a furnace is constructed in such a way to measure simultaneously the Seebeck coefficient and electrical conductivity of solid state

materials using two thermocouples and two current pins arranged in four-linear electrical terminals(Denner,2015; Netzsch, 2015). The carrier system contains a sample support which has two micro heaters (to generate a temperature gradient, ΔT between both ends of the sample), two current pins (outer probes) and two thermocouples (inner probes) (Figure 4). In SBA 458 Nemesis instrument (Denner, 2015), the distance between the current pins is 11.50 mm, while the distance between the thermocouples is 8.25 mm.

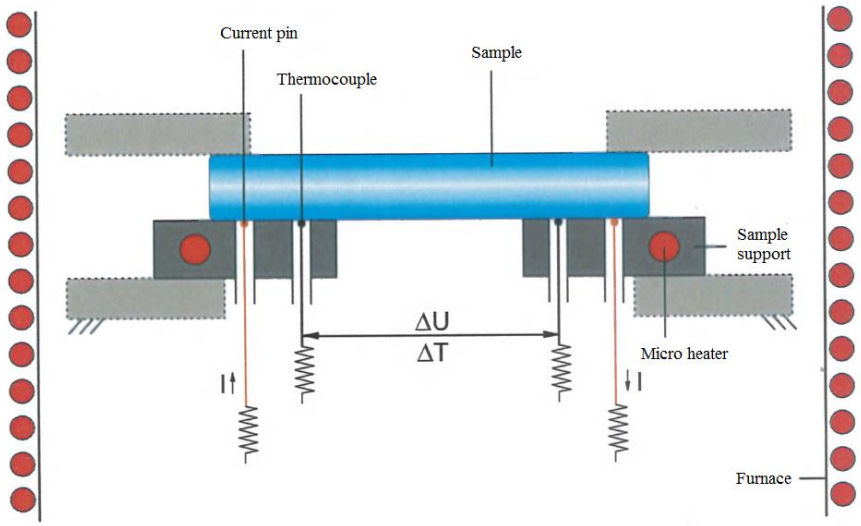

Figure 2. Simultaneous electrical conductivity and Seebeck coefficient measurement set up for the SBA 458 Nemesis instrument in the temperature range between room temperature and 700 °C(Denner, 2015).

3.2. Thermal Conductivity

The commonly used techniques for measuring the thermal conductivity of bulk materials include steady-state absolute method, comparative technique, laser flash diffusivity (LFD) method and transient plane source (TPS) method (Zhao et al,2016). In this work, LFD method was used. Laser flash method utilizes non-contact, non-destructive temperature sensing to achieve a high precision (Zhao et al, 2016). The LFD method was first introduced by Parker *et al* in 1961 and has remained a preferred method for researchers of thermophysical properties of materials and is the most common method for the determination of thermal conductivity of bulk ceramics (Boston et al, 2016). A typical arrangement of LFD method is shown in Figure 5.It uses instantaneous heat source (laser or xenon flash) to heat up the sample's front side, and a high infra-red (IR) detector to measure the time-dependent temperature rise at the rear (back) side (Zhao et al, 2016). Thermal diffusivity values are computed from the temperature rise versus time data curve (Figure 5b). The higher the

thermal diffusivity of the sample, the faster the heat transfer and temperature rise on the rear side. The heat conduction is one dimensional with the presumption that no lateral heat loss occurs.

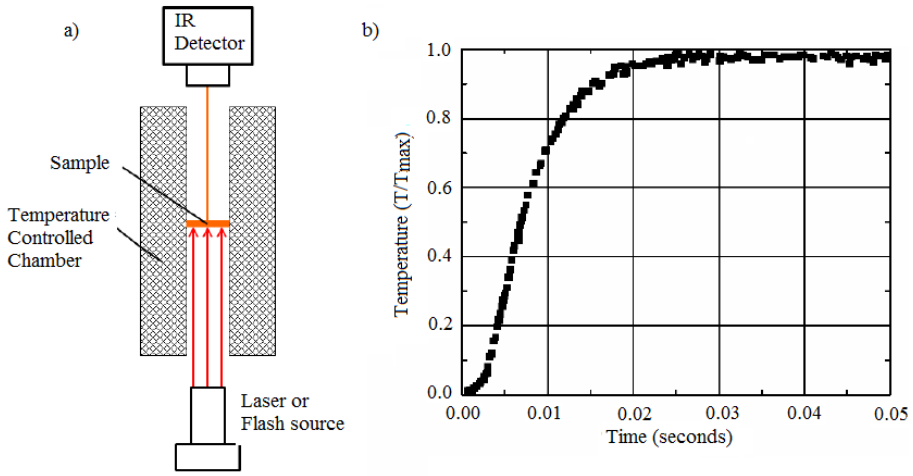

Figure 3 (a) Schematic measurement set up for the laser flash diffusivity (LFD) method. (b) An exemplary illustration of a measured time-dependent temperature rise data curve (Zhao et al, 2016).

The thermal conductivity (k) measurements were performed using a thermal property analyser (AnterFlashline TM 3000, Pittsburgh, PA 15235, USA) with High Speed Xenon Discharge (HSXD) pulse source and IR furnace operated with nitrogen gas. A square La+Sm doped $SrTiO_3$ sample of 10 x 10 mm with ~ 1.5 mm thickness was prepared for the measurements. The density of the sample measured using Archimedes method was keyed into the program software. The sample was cleaned with isopropanol, coated with graphite aerosol on both sides and allowed to dry. The prepared sample and a thermographite reference material were placed in different sample holders and positioned on a sample chamber (carousel) aligned with graphite foil located in the furnace. Thermographite is noted for its stability and well documented thermophysicalproperties, hence it is used as a common reference material in LFD method.

As the furnace was heated, it followed predetermined temperature steps (room temperature to 700 ^{o}C). At each temperature, the sample surface (front side) was irradiated with energy pulse from the HSXD. The energy pulse in turn resulted in a homogeneous temperature rises at the sample surface. The resulting temperature rise of the sample rear surface was measured by a high speed IR detector. Thermal diffusivity and specific heat values of the samples were then evaluated from the time-dependent temperature rise data (signal) generated. Combining the

thermal diffusivity (α), specific heat capacity (C_p) and density (ρ) values, the total thermal conductivity (k) of the sample was calculated using the following equation with expanded uncertainty of ± 4 % for AnterFlashline thermal properties analyser:

$$k(T) = \alpha(T) * C_p * \rho(T) \qquad 4.0$$

where T is the predetermined temperature.

The determination of k using the laser flash system is the most significant source of error for the calculation of thermoelectric figure of merit. This is obvious because, measurement of k involves the integration of density and specific heat capacity data which have their own errors. To minimize the uncertainty resulting from density measurement via Archimedes principle, use of high density samples are encouraged. Porous samples can absorb the liquid, leading to an overestimation of the density values (Borup et al, 2015). In as much as graphite coating of the sample prior to measurement is pertinent to ensure excellent emissivity and absorption of the laser impulse and detector signal (Neidhardt , 2014; Borup et al, 2015), thin coatings are required for reliable diffusivity data. Excess graphite coatings of samples could cause errors [29]. In controlling the errors inherent in C_p measurement, the thickness of the sample should be thin enough to allow the value of $t_{1/2}$ to be ≤ 0.3 s, thereby minimizing heat losses (Boston et al, 2016)[3]. $t_{1/2}$ is the time required of the temperature to increase to half-maximum, and it is utilized in calculating the thermal diffusivity (Borup et al, 2015). With these measures in place, the errors in ZT can be minimized. However, the accuracy and percent errors associated with the individual measurements of σ, S and k lead to a final uncertainty of ±14 % in ZT.

3.3. Dimensionless figure of merit

Dimensionless figure of merit, ZT describes the material's performance, hence is a prerequisite for a good thermoelectric material. It is a measure of the competition between electronic transport (power factor) and thermal transport (total thermal conductivity) in a material (Dehkordi, 2014). ZT is a combination of both electrical (Seebeck coefficient and electrical conductivity) and thermal (thermal conductivity) contributions to the properties of the thermoelectric materials and is given as:

$$ZT = \frac{S^2 \sigma T}{K} \qquad 5.0$$

where S is the Seebeck coefficient, σ is the electrical conductivity, T is the absolute temperature, and k is the total thermal conductivity. The higher the ZT, the better the efficiency of the thermoelectric materialsgenerate power high temperatures.

4.0. CONCLUSION

Perovskite-based materials have demonstrated significant potential for high-temperature thermoelectric power generation due to excellent thermal stability, oxidation resistance, structural versatility and environmental compatibility.

A comprehensive structural characterization using particle size analysis (PSA), thermogravimetric analysis (TGA), x-ray diffraction (XRD), scanning electron microscopy (SEM), and energy dispersive x-ray spectroscopy (EDX) provides critical information on powder characteristics, thermal behavior, crystal structure, microstructure, and elemental composition. These structural features strongly influence charge carrier transport and phonon scattering mechanisms that govern thermoelectric efficiency (Brown, 2001; Cullity and Stock, 2001; Goldstein et al, 2018). Thermoelectric characterization, including measurements of the Seebeck coefficient, electrical conductivity, thermal conductivity, and figure merit, is essential for evaluating material performance and understanding transport behavior at elevated temperatures.

Overall, the integration of advanced structural and thermoelectric characterization techniques provides a strong foundation for the development of efficient perovskite-based thermoelectric materials. Continued research in defect engineering, nanostructuring, and compositional optimization is expected to further enhance their performance and accelerate their application in sustainable high-temperature waste heat recovery and power generation systems.

REFERENCES

1. Anthony R. West. (2014). *Solid State Chemistry and its Applications*, Second Edi. West Sussex: Willey and Sons Limited.
2. Boston,R., Schmidt,W.L., Lewin, G.D., Iyasara, A.C., Lu, Z., Zhang, H., Sinclair, D.C., & Reaney, I.M. (2016). Protocols for the fabrication, characterization, and optimization of n-type thermoelectric ceramic oxides. *Chem. Mater.*,29(1), 265–280.
3. Brown, M.E. (2001). Introduction to thermal analysis: Techniques and applications (2nd ed.). Springer
4. Cullity, B.D., & Stock, S.R.(2001). Elements of x-ray diffraction (3rd ed.). Prentice Hall.
5. David Brandon & Wayne D. Kaplan. (2008). *Microstructural characterization of*

Materials, Second Edition, New Jersey: Wiley and Sons.

6. Dongliang Zhao, Xin Qian, Xiaokun Gu, Saad Ayub Jajja, & Ronggui Yang. (2016). Measurement Techniques for Thermal Conductivity and Interfacial Thermal Conductance of Bulk and Thin Film Materials. *J. Electron. Packag.*, 138(4), 1–64.
7. Fabia Neidhardt. (2014). When and How Must Samples Be Coated During LFA Measurements. *Appl. Note-Netzsch*, 1–4.
8. Fawcett, T.G., Needham, F., Crowder, C.E., & Kabekkodu, S. (2009). Advanced Materials Analysis using the Powder Diffraction File, in *10th National Conference on x-ray Diffraction and ICDD Workshop*, 1–3.
9. Goldstein, J.I., Newbury, D.E., Michael, J.R., Ritchie, N.W., Scott, J.H., & Joy, D. C. (2018). Scanning electron microscopy and x-ray microanalysis (4thed.). Springer.
10. Heremans, J.P., Dresselhaus, M.S., Bell, L.E, &Morelli, D.T. (2013).When thermoelectrics reached the nanoscale. Nature Nanotechnology, 8(7), 471-473.
11. Hongchao Wang & Chunlei Wang. (2013). Thermoelectric properties of Yb-doped $La_{0.1}Sr_{0.9}TiO_3$ ceramics at high temperature. *Ceramic International*, 39(2), 941–946.
12. Inform White Paper (2012), A Basic Guide to Particle Characterization. *Malvern Instruments Ltd.*, 1–26.
13. Johannes De Boor & Volker Schmidt. (2011) "Efficient thermoelectric van der Pauw measurements," *Appl. Phys. Lett.*, vol. 99, no. 2, pp. 5–7, 2011.
14. Kasper A. Borup, Johannes De Boor, Heng Wang, Fivos Drymiotis, Franck Gascoin, Xun Shi, Lidong Chen, Mikhail I. Fedorov, Eckhard Müller, Bo B. Iversen, & Jeffrey G. Snyder. (2015). Measuring thermoelectric transport properties of materials," *Energy Environ. Sci.*, 8(2), 423–435.
15. Myscope. (2014). *Introduction to Scanning Electron Microscopy*. Australian Microscopy & Microanalysis Research Facility, www.ammrf.org.au/MyScope.
16. Netzsch. (2015). *Simultaneous Determination of Seebeck Coefficient and Electrical Conductivity-SBA 458 Nemesis*. Germany: NETZSCH-Geratebau GmbH.
17. Parker, W.J., Jenkins, R.J., Butler, C.P., Abbott, G.L. (1961). Flash method of determining thermal diffusivity, heat capacity, and thermal conductivity. *J. Appl. Phys.*,32(9), 1679–1684.
18. Pena, M.A., &Fierro, J.L.G. (2001).Chemical structures and performance of perovskite oxides. Chemical Reviews, 101(&), 1981-2018.
19. PerkinElmer. (2010). *Thermogravimetric Analysis (TGA : A Beginner's Guide*. Waltham, USA: Perkin Elmer Inc.

20. Rahaman, M.N. (2003). Ceramic processing and sintering (2nded.). Marcel Dekker.
21. Rowe, D.M. (2006). Thermoelectrics handbook: Macro to nano. CRC Press.
22. Saulius Graulis, Daniel Chateigner, Robert T. Downs, Yokochi, A.F.T, Miguel Quirós, Luca Lutterotti, Elena Manakova, Justas Butkus, Peter Moeck, & Armel Le Bail.(2009). Crystallography Open Database - An open-access collection of crystal structures. *J. Appl. Crystallogr.*, 42(4), 726–729.
23. Snyder, G.J., &Toberer, E.S. (2008).Complex thermoelectric materials. Nature Materials, &(2), 105-114.
24. Thomas Denner.(2015). *Operating Instructions SBA 458 Nemesis.pdf*. Wittelsbacher, Germany: NETZSCH-Geratebau GmbH, http://www.netzsch-thermal-analysis.com.
25. Valdes, L.B. (1954). Resistivity Measurements on Germanium for Transistors, in *Proceedings of I-R-E*, 42, 420–427.
26. Valentin Garcia-Vazquez. (2017). Biased four-point probe resistance.*Rev. Sci. Instrum.*, 88(11).
27. Wenner, F. (1916). A method of measuring earth resistivity. *Bull. Bur. Stand.*,12(4), 469.